Front. Struct. Civ. Eng. 2025, 19(6): 933–945
https://doi.org/10.1007/s11709-025-1186-3

RESEARCH ARTICLE

Performance-based approach to characterize external sulfate attack for reactive powder concrete

Umut BAKHBERGEN[a], Chang-Seon SHON[a*], Dichuan ZHANG[a], Jong Ryeol KIM[a], Jenny LIU[b]

[a] *Department of Civil and Environmental Engineering, School of Engineering and Digital Sciences, Nazarbayev University, Astana 010000, Kazakhstan*

[b] *Department of Civil, Architectural, and Environmental Engineering, Missouri University of Science and Technology, Rolla, MO 65409-0030, USA*

[*] *Corresponding author. E-mail: chang.shon@nu.edu.kz*

ABSTRACT Reactive powder concrete (RPC) is a relatively new type of high-performance concrete, offering enhanced load-bearing capacity, mechanical strength, and durability. The enhanced microstructural density of RPC with the incorporation of reinforcing fibers significantly increases its resistance to durability challenges, particularly against external sulfate attack (ESA). However, conventional laboratory testing methods for evaluating the resistance of RPC to ESA are limited. Hence, a new performance-based approach was developed to evaluate the durability of RPC exposed to ESA. Expansion of nine RPC mixtures designed by Taguchi L9 orthogonal array method with four factors (steel fiber content, water-to-binder ratio (w/b), silica fume content, and sodium sulfate (Na_2SO_4) concentration) at three different temperatures (20, 40, and 60 °C) was used to calculate the reaction rate constant based on the first order chemical reaction kinetics. This mathematical model was rearranged to determine the activation energy (E_a), minimal energy required to initiate the ESA reaction, of RPC mixtures that were used to evaluate the performance of RPC mixtures exposed to ESA. The threshold value of E_a was determined from the correlation between Na_2SO_4 solution concentrations and the E_a values of RPC mixtures. It was concluded that the model-defined parameters provide valuable insights to characterize the ESA durability of RPC.

KEYWORDS performance-based approach, reactive powder concrete, external sulfate attack, reaction rate constant, activation energy

1 Introduction

The demand for high-performance concrete in modern construction continues to grow due to its critical role in enhancing structural performance and extending service life. Among these advanced materials, reactive powder concrete (RPC), also known as ultra-high-performance concrete, has emerged as a cutting-edge solution, offering superior load-bearing capacity [1], mechanical strength [2], and durability [3]. These features are primarily attributed to RPC's densely packed microstructure achieved by low water-to-binder ratio (w/b) [4], removal of coarse aggregate [3], improvement of the fine aggregate packing degree [5], and the incorporation of reinforcing fibers [6] and pozzolanic materials [7], which significantly improve its resistance to degradation, particularly under harsh environmental conditions such as external sulfate attack (ESA) [8].

ESA is a degradation process associated with exposing concrete structures to sulfate-rich environments [9]. The performance of concrete subjected to ESA is primarily influenced by two key factors. The first is the inherent properties of the concrete, which are determined by its mixture design [10,11]. Research generally highlights that the dense microstructure of RPC enhances its durability against ESA by minimizing sulfate ingress [12,13]. Conversely, some studies suggest that cement-based materials with relatively high porosity can better accommodate the expansive products of ESA reactions, thereby experiencing less severe or delayed sulfate-

Article history: Received Jul 7, 2024; Accepted Feb 27, 2025

induced damage [14,15]. The second factor is the exposure conditions, including the type of sulfate, its concentration, and the temperature. For instance, Akiiz et al. [16] observed that cement mortars exhibited negligible expansion at sodium sulfate (Na_2SO_4) concentrations below 0.18 mol/L. However, at higher Na_2SO_4 concentrations, the rate of concrete expansion shifts markedly after a specific duration, referred to as the "critical time" point. Consequently, the expansion-time relationship of concrete exposed to ESA is nonlinear. Additionally, temperature plays a critical role in determining the durability of concrete under sulfate exposure, significantly influencing the progression and severity of ESA [17,18]. Traditional laboratory-based methods are often limited in their ability to capture the complex chemical and physical interactions involved in sulfate resistance. The durability assessment of RPC under ESA remains challenging.

Numerous studies have sought to model the ESA process by incorporating one or more of its key aspects, including transport [19], chemical reactions [20], expansive forces [21], and mechanical response [22]. The transport process involves the penetration of sulfate ions into the concrete matrix. While the chemical reactions associated with ESA in concrete are complex, they generally adhere to the principles of chemical reaction kinetics, with unexposed concrete typically in an equilibrium state [23]. The ingress of sulfate ions disrupts this equilibrium, leading to damage caused by Na_2SO_4 through the formation of ettringite and gypsum. These compounds precipitate within the concrete matrix, generating expansive forces [21,24].

Additionally, prolonged exposure to sulfate-rich environments can dissolve calcium silicate hydrate, a critical component for concrete's strength, thereby contributing to structural degradation [20]. This degradation eventually manifests macro-cracking and a significant loss of strength in the later stages of sulfate exposure [13,17]. The volume change theory and the crystallization pressure theory are the most widely accepted explanations for the effects of ESA on concrete [21]. According to the volume change theory, expansion occurs due to the accumulation of ESA reaction products within the porous structure of the concrete [18]. Conversely, the crystallization pressure theory attributes the pressure to the buildup of ettringite within the material [24,25]. Concrete's mechanical response encompasses internal and external damage caused by ESA. A combination of mixture design parameters and exposure conditions influences the rate and severity of this response. Notably, exposure to sulfates does not inherently result in mechanical damage, as other factors significantly affect the occurrence and progression of such responses [18,20]. Hence, developing a kinetics-based model to assess ESA-induced damage in RPC is paramount.

This study introduces a performance-based ESA model for RPC that incorporates the chemical reaction kinetics of ESA, as reflected in the expansion behavior of RPC under three varying sulfate concentrations and temperatures. The proposed model provides two interrelated evaluation criteria: the reaction rate constant and activation energy, both of which are reliable indicators for predicting RPC performance under ESA conditions. To ensure the validity of these model-defined parameters, they are compared against the initial properties of RPC mixtures, which serve as indicators of their microstructural characteristics.

2 Research scope and experimental program

2.1 Research scope

As illustrated in Fig. 1, the structural and construction materials group at Nazarbayev University has researched RPC under sulfate environments. Sulfate-rich soils, which are prevalent throughout Kazakhstan and Central Asia, pose a significant risk of ESA to concrete structures due to the migration of sulfate ions into the material. Recognizing this potential hazard, the research team undertook a series of studies on RPC, focusing on its performance under sulfate-rich conditions and varying temperature environments. The RPC project included 1) Phase I: optimizing mixture parameters to obtain good physical and mechanical properties of RPC under ESA using the Taguchi method [15], 2) Phase II: assessing compressive strength, modulus of rupture, absorption, porosity, microstructure, and durability of RPC subjected to three different Na_2SO_4 concentrations [2], and 3) Phase III: developing a performance-based approach to characterize ESA in RPC.

As a Phase III study, this paper focuses on developing a performance-based approach to characterize ESA for RPC. The performance of RPC exposed to ESA cannot be adequately assessed solely by measuring length change as a percentage or relying on the 0.1% expansion threshold specified by ASTM C1012 [26]. A chemical reaction kinetics model has been developed to evaluate RPC's performance under varying temperatures and Na_2SO_4 concentrations to address this limitation. The sensitivity of RPC mixtures to ESA is quantified using the activation energy (E_a) parameter, derived through a kinetic approach. Furthermore, the study establishes a relationship between E_a, absorption capacity (AC), and permeability. Finally, a kinetics-based mathematical model determines the threshold Na_2SO_4 concentration required to initiate rapid ESA damage.

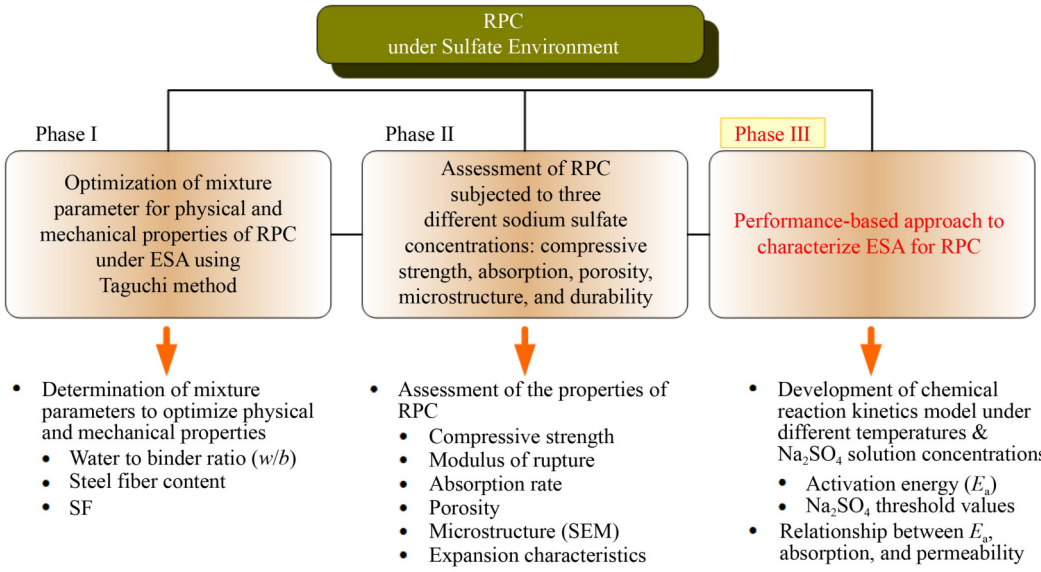

Fig. 1 Diagram of overall research scopes and experimental program.

2.2 Materials and mixture proportions

Table 1 presents the properties of ASTM Type I ordinary Portland cement (OPC) and silica fume (SF) used as binders for the RPC mixture. Locally available fine quartz sands with improved packing degree [5], as by properties shown in Table 2, were used as fine aggregate for the RPC mixture. Steel fibers with Φ0.16 mm and 13 mm length, Master Glenium ACE 430 superplasticizer (SP) with specific gravity 1.02, and ordinary tap water were also used to cast RPC specimens. Locally produced Na_2SO_4 of 98% purity was dissolved in deionized water to produce sulfate solutions of specified molar concentrations. Na_2SO_4 solutions were refreshed every three months.

Table 1 Properties of binder

Component	Cement	SF
Chemical composition (% mass)		
CaO	62.73	0.22
SiO_2	20.78	97.5
Al_2O_3	4.82	0.2
Fe_2O_3	3.95	0.5
SO_3	3.14	0.12
MgO	1.57	0.56
Na_2O	0.78	0.25
K_2O	–	0.56
Minerology		
C_3S	64	–
C_2S	15	–
C_3A	6	–
C_4AF	12	–
Physical properties		
Specific surface area (m^2/kg)	421	2300
Specific gravity	3.15	2.22
Loss on ignition	2.08	2.08

Table 2 Properties of aggregate

Property	Value
Packing degree, φ	0.6436
Size fractions (retained on sieve)	0.075, 0.150, 0.300
Weight ratio of larger grain size to smaller grain size, β	0.75
Absorption capacity, AC	5.16
Moisture content, MC	0.26
Apparent specific gravity, G_a	2.88

A total of 9 mixtures designed by L9 orthogonal array Taguchi design of experiments with four parameters (steel fiber content, w/b, SF content, and Na_2SO_4 concentration) at three levels were exposed to ESA at three different temperatures (20, 40, and 60 °C). The absolute volume method was used to quantify the mixture components of RPC mixtures. SP dosage varied to achieve a workability of (180 ± 40) mm under the ASTM C1437 [27]. Taguchi's design of experiments and mixture proportioning is given in Table 3.

2.3 Mixing procedure, casting specimen, and testing methods

A 5.6-L Hobart mortar mixer was used to complete the mixing of RPC samples by following the procedure. Cementitious materials (OPC and SF) were added to the mixer and dry mixed for 30 s. After that, 1/2 of the water was slowly poured into the mixer while continuously mixing for 90 s. Then, all sand and steel fibers were

Table 3 L9 orthogonal array Taguchi design of experiments and mixture proportioning

No.	Mixture ID	Steel fiber (% of aggregate by mass)		*w*/*b*		SF (% of cement by mass)		Na_2SO_4 concentration (conc) (mol/L)		Cement (kg/m^3)	Sand (kg/m^3)	SP (% of binder)
		mix design	L9 level	mix decide	L9 level	mix design	L9 level	mix design	L9 level			
1	0-0.16-15-0.35	0	1	0.16	1	15	1	0.35	1	1043	1155	6
2	0-0.20-20-1.05	0	1	0.2	2	20	2	1.05	2	1000	1002	3
3	0-0.24-25-3.15	0	1	0.24	3	25	3	3.15	3	960	851	2.5
4	1-0.16-20-3.15	1	2	0.16	1	20	2	3.15	3	1000	1139	6
5	1-0.20-25-0.35	1	2	0.2	2	25	3	0.35	1	960	987	4.5
6	1-0.24-15-1.05	1	2	0.24	3	15	1	1.05	2	1043	882	3
7	2-0.16-25-1.05	2	3	0.16	1	25	3	1.05	2	960	1124	8
8	2-0.20-15-3.15	2	3	0.2	2	15	1	3.15	3	1043	1019	4.5
9	2-0.24-20-0.35	2	3	0.24	3	20	2	0.35	1	1000	866	3

Note: Mixture 0-0.16-15-0.35 indicates 0% steel fiber, 0.16 *w*/*b*, 15% SF content, 0.35 mol/L Na_2SO_4 test solution concentration.

added and mixed for 60 s. Afterward, SP dissolved in the remaining 1/2 of water was introduced and mixed for 180 s. After stopping the mixer, the RPC accumulated on the side of the mixer was quickly scraped down, allowed to absorb water, and then made a stable mixture for 60 s. Finally, the last mixing was applied for (120 ± 60) s until a homogeneous RPC mixture was achieved.

The RPC mixtures were placed into molds immediately after the mixing. Improved compaction was achieved by placing the concrete in two layers with subsequent tapping with a rubber stick. Plastic sheets covered molds for 24 h to avoid water evaporation. Specimens from all 9 RPC mixtures satisfied ASTM C1012 [26] requirement in minimal compressive strength (20 ± 2) MPa before ESA exposure.

According to the ASTM C1012 testing method, 25 mm × 25 mm × 250 mm length change specimens were placed in their corresponding Na_2SO_4 solutions after demolding. Length change was measured every week up to 8 weeks, every 2 or 3 weeks up to 26 weeks (6 months), and monthly up to 52 weeks (1 year). The average value of length change was calculated as in Eq. (1) based on the data from 3 to 6 samples measured for each mixture.

$$\Delta L = \frac{L_x - L_i}{L_g} \times 100, \tag{1}$$

where L_x = comparator reading of specimen at x age—reference bar comparator reading, L_i = initial comparator reading of specimen—reference bar comparator reading, at the same time L_g = nominal gauge length, or 250 mm.

The sorptivity of RPC mixtures, also known as an absorption rate, was determined per the ASTM C1585 [28] procedure with Φ100 mm and 50 mm length test samples. Absorption of RPC mixtures was calculated based on the testing data as given in Eq. (2).

$$I = \frac{m_t}{a \times d}, \tag{2}$$

where I = absorption, m_t = change in specimen mass in grams (g) at time t, a = the exposed area of the specimen in mm^2, and d = the density of water in g/mm^3.

The initial (30 s to 24 h measurement) and secondary (1 to 7 d measurement) sorptivity (mm/s$^{1/2}$) is determined by the slope of the best-fit line for the absorption (I) versus square root of time ($\sqrt{t}$) plot.

The volume of permeable voids, referred to as the initial permeability of concrete, was determined using Φ100 mm and 200 mm length samples as specified by the ASTM C642 standard test method [29].

3 Test results for absorption and expansion characteristics of reactive powder concrete

3.1 Absorption of reactive powder concrete mixtures

Figure 2 shows the absorption of the RPC mixtures. The highest absorption, both initial and secondary, is observed for Mixture 6 (1-0.24-15-1.05) which has the highest *w*/*b* and lowest SF content, followed by Mixture 7 (2-0.16-25-1.05) which, in contrast, has the lowest *w*/*b* and the highest SF content. On the other hand, the lowest initial and secondary absorption levels were for Mixture 8 (2-0.20-15-3.15) and Mixture 5 (1-0.20-25-0.35). Both mixtures had medium *w*/*b* and different SF contents. Therefore, it can be stated that since adding SF increases the water demand of the RPC mixture, high SF content at low *w*/*b* results in the high ingress of water (and potentially of the sulfate solution).

A high *w*/*b* combined with low SF content in the RPC mixture leads to a less dense microstructure, as water can easily penetrate the concrete pores. When the *w*/*b* ratio is optimized at 0.20, SF actively participates in the pozzolanic reaction, enhancing the microstructure of RPC. However, excessive SF content may function merely as a filler rather than contributing to the reaction

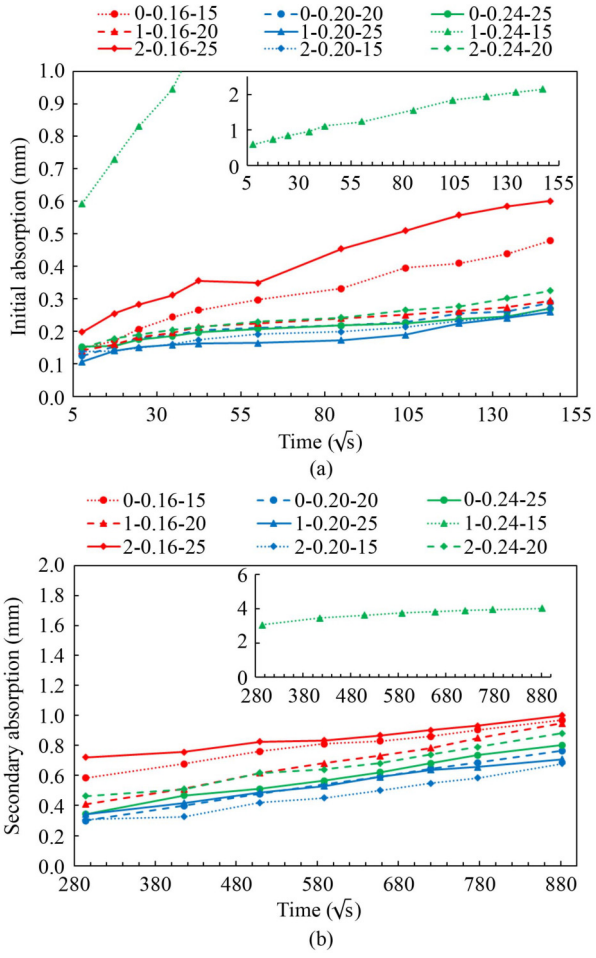

Fig. 2 Absorption of RPC mixtures: (a) initial; (b) secondary.

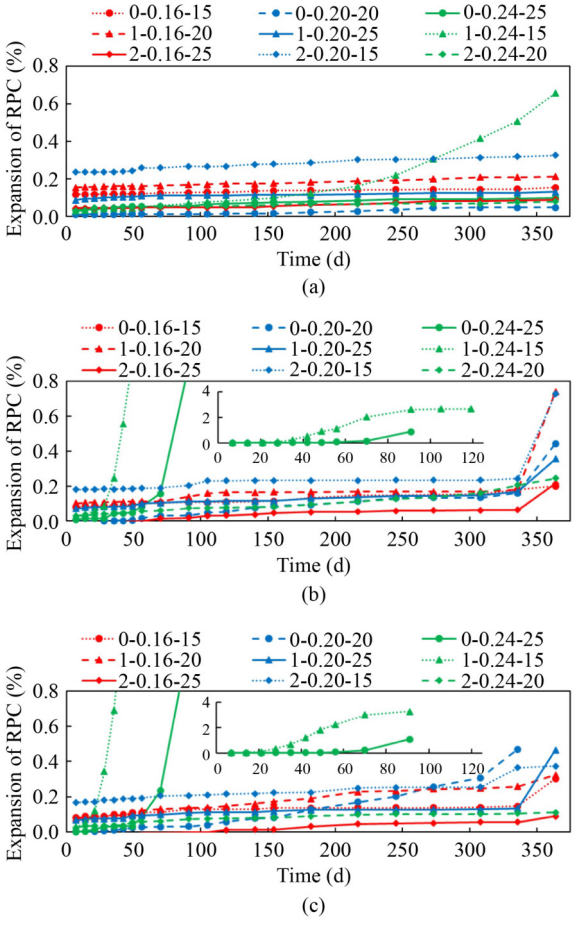

Fig. 3 Length change of RPC mixtures: (a) 20 °C; (b) 40 °C; (c) 60 °C.

[3,30]. It is important to note that the initial absorption rate of water is significantly higher than the secondary absorption rate, as the saturation of concrete pores inhibits further water ingress [14,31]. The slopes of the initial and secondary absorption rates are used to calculate the initial and secondary sorptivity, respectively, which will later serve to validate the model-defined parameters.

3.2 Expansion of reactive powder concrete mixtures exposed to external sulfate attack

The length change of RPC mixtures was measured for up to 1 year, as shown in Fig. 3. Irrespective of the exposure temperature, all RPC mixtures, except for Mixture 6 (1-0.24-15-1.05) and Mixture 3 (0-0.24-25-3.15), exhibit similar expansion levels, remaining below 0.2%. According to ASTM C1012 [26], concrete with less than 0.1% expansion after one year of exposure demonstrates moderate resistance to sulfate attack. As depicted in Fig. 3(a), all tested RPC mixtures, except for Mixture 6 (1-0.24-15-1.05), Mixture 8 (2-0.20-15-3.15), and Mixture 4 (1-0.16-20-3.15), fall within this category of moderate ESA resistance. The standard test for ESA resistance involves exposing concrete to a 5% (0.35 mol/L) Na_2SO_4 solution at ambient temperature. However, standard conditions typically do not induce significant expansion in RPC [15,32]. Notably, the Na_2SO_4 concentrations for mixtures exhibiting expansion exceeding 0.1% after one year of exposure at 20 °C were 1.05 and 3.15 mol/L—three and nine times higher than the standard concentration, respectively. Consequently, based on the length change observed in this study, it can be concluded that RPC demonstrates moderate to high resistance to ESA.

When high-temperature exposure to ESA is considered, the rate and extent of expansion in RPC mixtures increase substantially, as illustrated in Figs. 3(b) and 3(c). Mixture 3 (0-0.24-25-3.15) exhibited a length increase of approximately 1%, leading to the complete deterioration of all samples after 13 weeks (91 d) at both 40 and 60 °C. Similarly, Mixture 6 (1-0.24-15-1.05) experienced complete deterioration after 17 weeks (119 d) at 40 °C and after 13 weeks (91 d) at 60 °C. This macro-level physical response of RPC mixtures to relatively short-term ESA exposure suggests that ettringite formation may

have caused the degradation of calcium silicate hydrates (C-S-H) [18,33,34]. Notably, Mixture 6 displayed significant expansion levels at failure, reaching 2% at 40 °C and 3% at 60 °C.

First, these findings indicate that lower Na_2SO_4 concentrations can induce more severe expansion, likely due to the temperature-dependent solubility of Na_2SO_4 [34]. Secondly, the results highlight the influence of mixture design parameters on RPC's ESA resistance. Specifically, Mixture 6, which contains a higher steel fiber content and lower SF content, exhibited more significant expansion prior to failure. The reduced SF content may have mitigated the pore-filling effect, allowing pore spaces to act as "buffer zones" that accommodate ESA-induced expansive products over extended periods [14,35]. Conversely, Mixture 3's lower expansion prior to failure could be attributed to the detrimental effect of SF in reducing available pore space.

Figure 3 demonstrates that higher steel fiber content generally increases expansion in RPC mixtures. Steel fibers are primarily incorporated into RPC to enhance tensile strength and improve spalling behavior under failure conditions. However, their relatively coarse size compared to other constituents in RPC can disrupt the homogeneity of the concrete matrix [36,37]. Regardless of the exposure conditions, RPC mixtures with a *w*/*b* of 0.20 exhibit the least length change, followed by those with a *w*/*b* of 0.16. This suggests that increasing the *w*/*b* ratio, which raises porosity and permeability, facilitates sulfate ingress in RPC [6]. Additionally, an increase in SF content tends to reduce the expansion of RPC mixtures, particularly during the initial weeks of exposure. This reduction is attributed to the pore-filling effect of SF, which appears to be beneficial in the early stages of ESA exposure by preventing sulfate penetration into the pore spaces of the concrete.

4 Development of a performance-based model to assess external sulfate attack in reactive powder concrete

4.1 The process of model development

As highlighted in the previous section, accurately evaluating the ESA resistance of RPC under varying environmental conditions using standard assessment methods poses challenges. A new assessment model was developed to address this issue by utilizing the actual ESA expansion data of RPC obtained in this study. Since the expansion of concrete due to ESA is a temperature-activated process influenced by sulfate ion concentration, the proposed model offers a direct means to account for various factors affecting ESA performance. These factors include temperature, sulfate ion concentration, age, and mixture proportions, expressed in terms of performance-related parameters. The core approach in developing this performance-based model for ESA in RPC involves identifying a single parameter that captures the combined effects of mixture design and exposure conditions. This model functions as an indicator of sulfate-induced damage in RPC. It can be employed to identify the threshold value that triggers expansion or to enhance the interpretation of expansion data derived from existing test methods.

The process for developing the model is schematically illustrated in Fig. 4. The initial step involves using the expansion data of RPC (Fig. 5(a)) as a physical response factor representing ESA-induced damage. The expansion of RPC is influenced by key mixture design parameters, including steel fiber content, *w*/*b*, SF content, and exposure conditions such as the concentration and temperature of the sulfate solution. Furthermore, expansion is traditionally regarded as an indicator of sulfate-induced damage in the conventional ESA

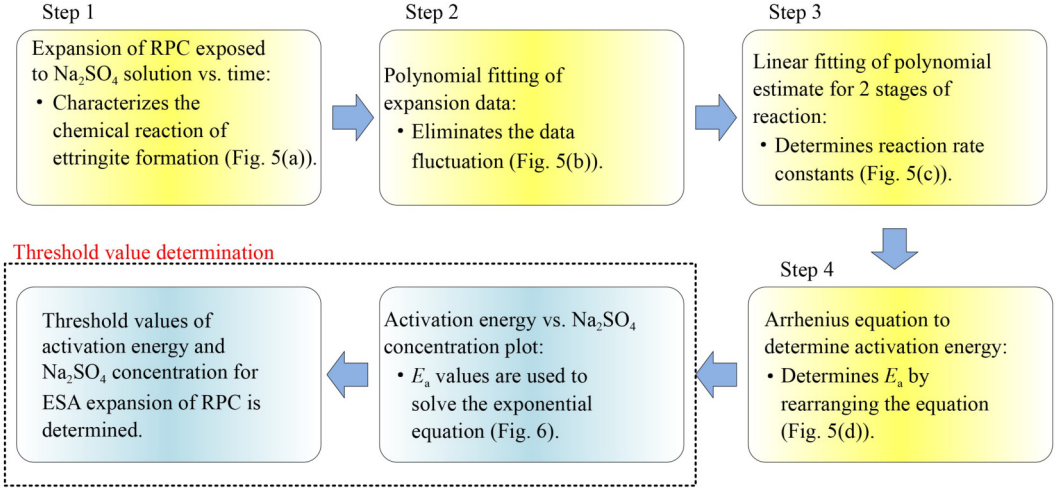

Fig. 4 Modeling ESA reaction in RPC: process map.

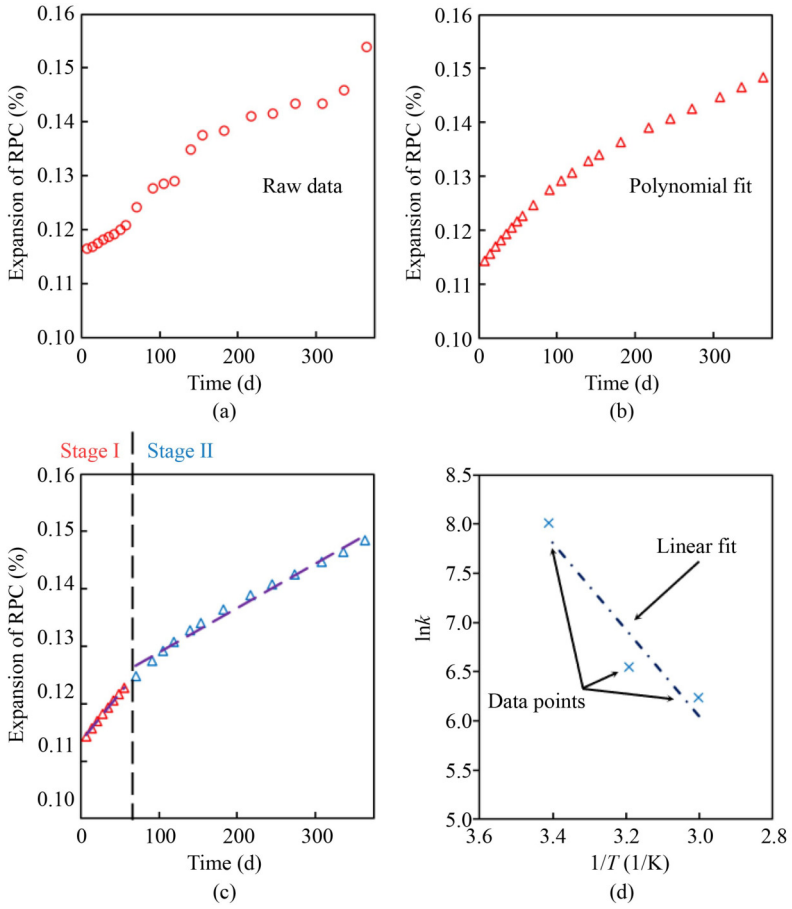

Fig. 5 Modeling ESA damage in RPC: (a) raw data; (b) polynomial fitting; (c) linear fitting of 2 stages of reaction; (d) activation energy calculation.

evaluation process, primarily due to ettringite formation.

In the second step, the expansion data from RPC mixtures is normalized using third-degree polynomial fitting, as illustrated in Fig. 5(b). It is proposed that ESA in concrete progresses through two distinct stages: the first involves an initial rapid expansion upon exposure to a sulfate-rich environment, and the second is marked by a slower, more steady expansion during long-term exposure [35]. To quantify these stages, the reaction rate constant is derived by performing a linear fit to the expansion-time graph, dividing it into two segments: the period up to 8 weeks and the period beyond 8 weeks. An example of this process is shown in Fig. 5(c).

In the third step, the kinetic law of chemical reactions is chosen to account for the ESA reaction chemistry. Hence, expansion is correlated to the ESA reaction kinetics by the first-order chemical reaction law as given in Eq. (3).

$$\log(\Delta L_t) = kt + \log(\Delta L_0), \tag{3}$$

where ΔL_t = length change of RPC at time t (%), ΔL_0 = ultimate length change of RPC, t = time, and k = reaction rate constant. Dimensional homogeneity of equation terms is ensured.

Therefore, the reaction rate constants for two stages of ESA reaction are determined for 9 RPC mixtures exposed to ESA at three different temperatures. The superposition principle is used to calculate the reaction rate constant of the ESA reaction for each mixture. Model-defined values are shown in Table 4.

In the fourth step, the reaction kinetics are analyzed with a chemical reaction's activation energy (E_a), as described by the Arrhenius function. The E_a represents the minimum energy required to initiate the reaction. Once initiated, the reaction proceeds rapidly until all reactants are depleted. Consequently, higher E_a values correspond to a slower reaction. ESA in concrete is influenced by the temperature and concentration of the sulfate as well as the mixture design parameters. Therefore, the concept of E_a serves as a valuable tool for evaluating the ESA reaction in concrete. The temperature-dependent Arrhenius equation, given in Eq. (4), is employed to establish a relationship between the reaction rate constant and the activation energy, providing a framework for understanding the influence of temperature on ESA progression.

$$k = A\mathrm{e}^{\frac{-E_a}{RT}}, \tag{4}$$

Table 4 Reaction rate constant and activation energy values of ESA damage reaction in RPC mixtures

No.	Mix ID	Reaction rate constant ($\times 10^{-4}$ d^{-1})			Activation energy (kJ/mol)
		Temperature 20 ℃	Temperature 40 ℃	Temperature 60 ℃	
1	0-0.16-15-0.35	2.55	6.52	13.03	3.18
2	0-0.20-20-1.05	2.05	21.58	21.08	1.34
3	0-0.24-25-3.15	4.56	326.81	397.07	0.08
4	1-0.16-20-3.15	3.09	30.07	13.89	0.54
5	1-0.20-25-0.35	3.31	14.32	19.60	2.02
6	1-0.24-15-1.05	23.54	409.84	573.75	0.06
7	2-0.16-25-1.05	2.21	12.62	6.60	1.48
8	2-0.20-15-3.15	6.21	25.71	11.97	0.55
9	2-0.24-20-0.35	3.78	11.47	7.39	2.22

where A = pre-exponential factor, R = universal gas constant, T = absolute temperature, and E_a = activation energy for the ESA reaction.

Rearranging Eq. (4), as shown in Eq. (5), by taking the natural logarithms from both sides allows us to find the as the slope of the line when the natural logarithm of reaction rate is plotted versus the reciprocal of temperature multiplied by a universal gas constant.

$$\ln(k_t) = \frac{-E_a}{R} \times \frac{1}{T} + \ln A. \tag{5}$$

An example of linear fitting to find the activation energy is given in Fig. 5(d), while E_a values of 9 RPC mixtures are shown in Table 4.

In the final steps, the threshold value of E_a and Na_2SO_4 concentration required to initiate the damage upon ESA exposure of RPC is determined. The detailed methodology is elaborated in Subsection 4.2.

4.2 Threshold value of external sulfate attack damage reaction in reactive powder concrete

E_a was correlated with sulfate concentration to minimize potential bias from various Na_2SO_4 concentrations used in this study along with the analysis of the RPC mixture design parameters. Figure 6(a) illustrates that increasing the steel fiber content significantly raises E_a at high sulfate concentrations (3.15 mol/L). Conversely, this trend is not observed at lower sulfate concentrations, and the highest E_a values are achieved in mixtures without fibers. This suggests that the homogeneity of the RPC microstructure is advantageous only under low sulfate concentration conditions, as it effectively blocks sulfate ingress into the pores. In more aggressive environments with higher sulfate concentrations, however, the ingress of sulfate into a less homogeneous microstructure allows for accumulating expansive products in the pores, making high fiber content more beneficial. Additionally, the fibers in RPC contribute to tensile strength, which becomes crucial in mitigating microstructural stresses induced by ESA reaction products [18,38]. Thus, while fiber content may have limited influence at low sulfate concentrations, it plays a vital role in enhancing RPC performance under more severe exposure conditions.

Figure 6(b) illustrates that increasing the w/b reduces the E_a of RPC mixtures regardless of the solution concentration. The reduction in E_a becomes particularly pronounced when w/b increases from 0.20 to 0.24. In contrast, a low w/b ratio is beneficial for RPC durability. Low w/b is advantageous for RPC when its strength and durability are considered: The lower w/b, the higher the strength and the lesser permeability. This leads to a high E_a that indicates durable RPC to ESA.

Figure 6(c) shows that increasing the SF content decreases the E_a of RPC mixtures. Moreover, the reduction in E_a becomes more pronounced at higher sulfate concentrations. This trend suggests that the pore-filling effect of SF, while beneficial to densify the concrete, can make RPC mixtures with higher SF content more susceptible to expansion. By limiting the pore spaces, the pore-filling effect reduces the capacity of the matrix to accommodate stresses induced by expansive products, thereby increasing the vulnerability of the RPC to ESA [30,32].

Taguchi's orthogonal array principle was applied to compile all test results (Figs. 6(a)–6(c)) to generate the concentration versus activation energy plots of RPC mixtures, as illustrated in Fig. 6(d). This plot allows threshold values to be determined to initiate the ESA in RPC mixtures. In this regard, E_a is assumed to be dependent on the reactant concentration, as given in Eq. (6).

$$E_a = a + b \times \exp(-c \times conc.), \tag{6}$$

where a, b, and c = the coefficients of an exponential function and $conc.$ = Na_2SO_4 solution concentration.

Solving the given equation for all different mixture design conditions is possible. The values of the

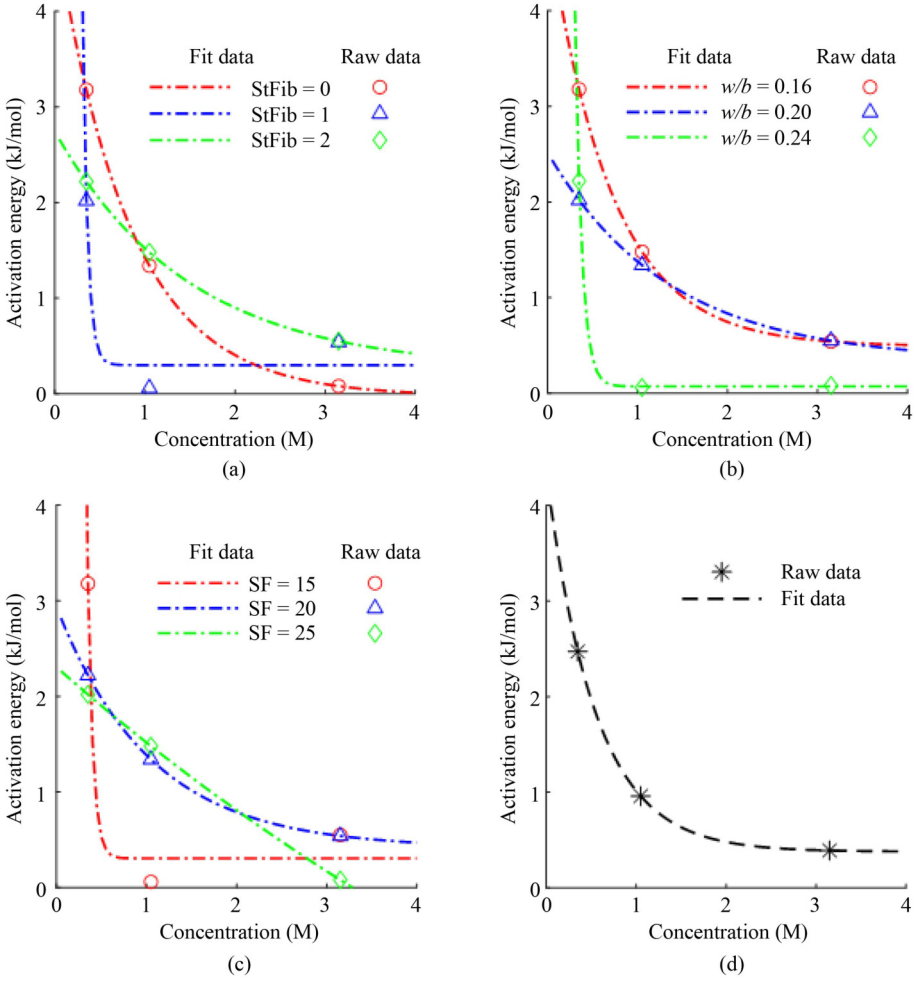

Fig. 6 Threshold value determination: activation energy vs. (a) steel fiber content; (b) *w*/*b*; (c) SF content; (d) Taguchi mean value.

Table 5 Equation coefficients

Variable parameter	Steel fiber content (%)			*w*/*b*			SF content (%)			Final values
	0	1	2	0.16	0.20	0.24	15	20	25	
a	−0.03	0.30	0.25	0.49	0.34	0.07	0.30	0.42	−5.56	0.38
b	4.91	844.35	2.49	4.43	2.18	215.18	1109.15	2.52	7.87	3.97
c	1.22	17.70	0.67	1.43	0.74	13.16	17.02	0.96	0.11	1.83

coefficients are given in Table 5. The threshold value is defined as a single parameter representing the energy level below which the ESA reaction in concrete cannot proceed kinetically. In other words, if the energy level of the concrete-sulfate system remains below this threshold, ESA-induced damage is unlikely to occur, irrespective of the sulfate concentration. The coefficient *a* in Eq. (6) represents the minimum E_a required to initiate the ettringite formation reaction in RPC.

However, applying Taguchi's orthogonality array principle for each mixture design parameter separately (steel fiber content, *w*/*b*, and SF content) yields the same single line in Fig. 6(d) with the solution given in Eq. (7).

$$E_a = 0.337 + 3.977 \times \exp(-1.831 \times conc.). \quad (7)$$

Based on this model, the threshold E_a value for ettringite formation in RPC is 0.377 kJ/mol. In other words, regardless of sulfate concentration, the reaction of ettringite formation will not occur in the Na_2SO_4 solution-RPC system for E_a values below 0.377 kJ/mol. Equation (6) can be used to estimate the E_a of ESA in RPC for any given Na_2SO_4 concentration. Additionally, Fig. 6 highlights a significant drop in E_a between concentrations > 1 mol/L and < 1.2 mol/L Na_2SO_4. This observation suggests that Na_2SO_4 concentrations below 1 mol/L cause minimal damage or significantly delay the onset of damage in RPC exposed to ESA.

5 Performance-based evaluation of external sulfate attack resistance of reactive powder concrete

5.1 Analyzing the effect of mixture design and exposure on model-defined parameters

Table 4 presents the calculated reaction rate constants and E_a for all RPC mixtures using the newly developed model. As noted earlier, the reaction rate constant and E_a are key indicators of the ESA susceptibility of RPC mixtures. The results show that Mixture 6 (1-0.24-15-1.05) and Mixture 3 (0-0.24-25-3.15) exhibit the highest reaction rate constants and the lowest E_a values, indicating low ESA resistance. In contrast, Mixture 1 (0-0.16-15-0.35) demonstrates the lowest reaction rate constant and the highest E_a, signifying the highest ESA resistance.

The reaction rate constants tend to increase with higher concentrations and temperatures of the test solution, which aligns with the principle that ion diffusion accelerates under such conditions, similar to other chemical reactions [39]. Additionally, an increased *w*/*b* ratio and reduced SF content negatively impact ESA resistance, as both factors elevate the reaction rate. However, no direct correlation is observed between steel fiber content and the reaction rate constant, as steel fiber is chemically inert and does not participate in the reaction. Therefore, the effect of fiber content on the ESA performance of RPC appears to be minimal.

Since E_a values are derived from reaction rate constants, the trends for both parameters are consistent. Nonetheless, the detailed influence of mixture design parameters on the E_a of RPC mixtures is discussed in the next section. Notably, the typical E_a value for ettringite formation is approximately 1 kJ/mol [40], and the E_a values determined by the model align with this benchmark, confirming its reliability. Based on the derived assessment parameters, Mixture 1 (0-0.16-15-0.35), Mixture 9 (2-0.24-20-0.35), and Mixture 5 (1-0.20-25-0.35) are identified as having high ESA resistance.

5.2 Correlating model-defined parameters and initial properties of reactive powder concrete

Figure 7 compares RPC mixtures' reaction rate constant values with their initial and secondary sorptivity values measured before ESA exposure. The two parameters exhibit a direct proportional relationship, indicating that mixtures with higher sorptivity levels tend to have higher reaction rate constants. Notably, the correlation between initial sorptivity and the first-stage reaction rate constant is more pronounced. This observation suggests that ESA-induced damage in RPC, particularly during the early stages, is governed by the ability of its pore structure to resist sulfate ingress [34,39]. However, at later stages, the damage appears to be influenced by the capacity of the pore spaces to act as a "buffer," accommodating expansive products without inducing significant microstructural stresses [14,35]. This distinction highlights the dual role of pore structure in controlling ESA progression over time.

Another initial property, RPC's permeability, was analyzed in relation to E_a, as shown in Fig. 8. Although a few exceptions were observed (e.g., Mixtures 1-0.20-25 and 2-0.20-20), E_a is generally inversely proportional to the permeability of RPC mixtures. For instance, in mixtures without steel fibers, E_a decreases as permeability increases. This trend highlights that mixtures with higher *w*/*b* exhibit greater porosity, allowing sulfate ions to migrate more easily into the concrete. Consequently, ettringite forms more rapidly and frequently, inducing expansion. It is important to note that in this study, the concept of E_a represents the minimum energy required to initiate ESA damage. As such, lower E_a values indicate a faster ESA reaction, aligning with the observed correlation between permeability and ESA susceptibility.

Moreover, RPC mixtures containing 1% and 2% steel fibers also follow the same trend of an inverse relationship between E_a and permeability, with exceptions such as Mixture 5 (1-0.20-25) and Mixture 9 (2-0.20-20). While E_a values differ due to variations in mixture proportions, Mixture 9 (2-0.24-20) stands out for its higher E_a despite having the highest permeability among mixtures with 2% steel fibers. This anomaly may be explained by the lower expansion observed in Mixture 9, which leads to its higher E_a.

Based on both traditional testing methods and the proposed performance-based model, Mixture 9, with a design comprising 2% steel fiber content, *w*/*b* of 0.24, and 20% SF content, emerges as the most durable option. Its superior performance can be attributed to its ability to limit expansion under ESA conditions, as expansive products are likely to accumulate within voids without causing significant damage. This finding highlights the effectiveness of its mixture design in enhancing durability against sulfate-induced damage. The clear correlation between model-defined parameters, such as E_a, and initial RPC properties like permeability further validates the model's reliability. Hence, the proposed performance-based approach for characterizing ESA in high-performance concretes like RPC proves beneficial. It effectively identifies the more sensitive and vulnerable mixtures to ESA, providing valuable insights for optimizing RPC mixtures to enhance durability.

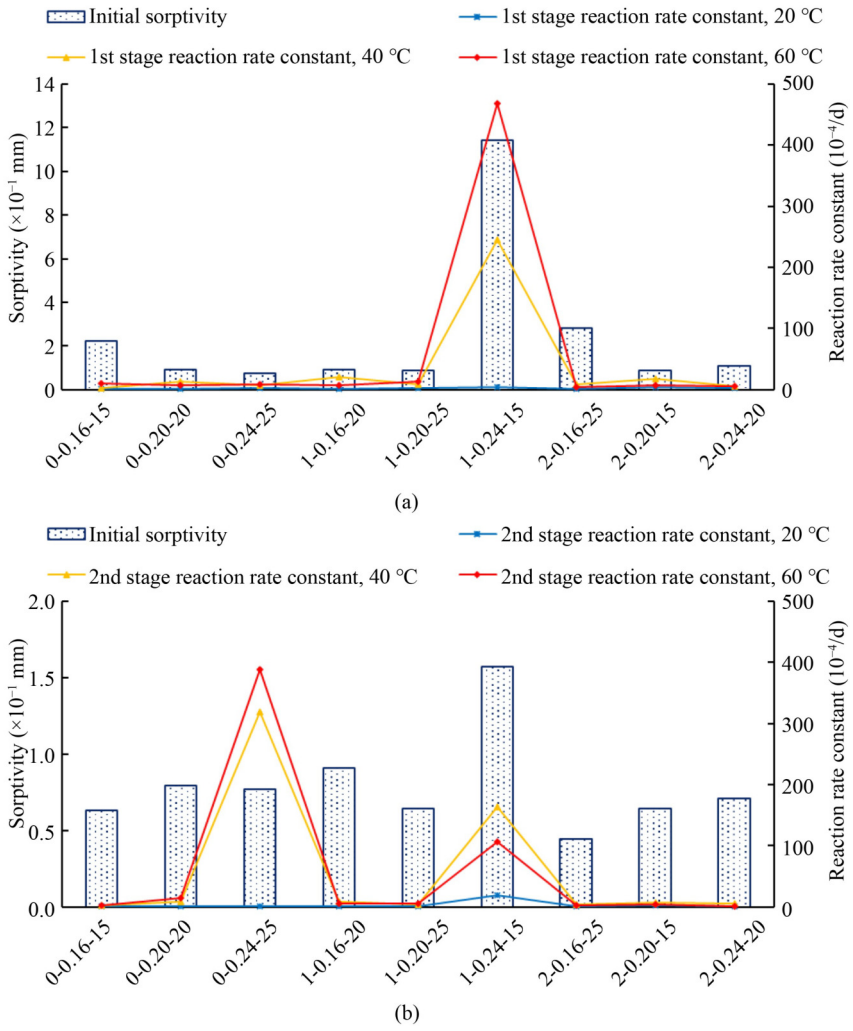

Fig. 7 Correlating reaction rate constants to sorptivity of RPC: (a) 1st stage and initial; (b) 2nd stage and secondary.

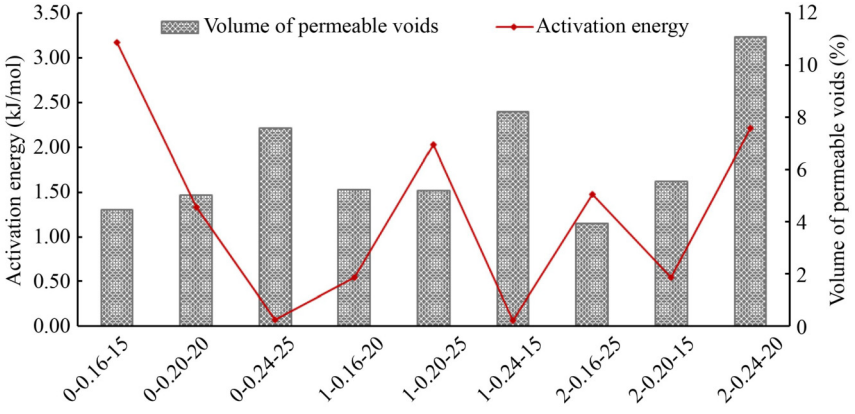

Fig. 8 Correlating activation energy to volume of permeable voids in RPC.

6 Conclusions

This study introduced a novel performance-based model for evaluating the resistance of RPC to ESA, addressing the limitations of conventional methods that fail to capture the superior characteristics of RPC adequately. The total of 9 RPC mixtures, designed using the Taguchi method, were tested following ASTM C1012 standards, and expansion data were analyzed using reaction kinetics and the Arrhenius equation to calculate activation energy (E_a). The findings reveal that ESA in RPC progresses in two distinct stages: the early-stage damage is governed by

the pore structure's ability to resist sulfate ingress, while later-stage performance is influenced by the capacity of pore spaces to buffer expansive products without inducing stress. The study identifies E_a as a critical parameter, establishing a threshold value of 0.377 kJ/mol, below which ESA reactions are kinetically inhibited. This threshold highlights the model's ability to predict ESA performance, emphasizing its practical utility in designing more durable RPC mixtures.

The results underscore the significant influence of mixture design on ESA resistance of RPC. Mixtures with lower *w*/*b* and optimized SF content demonstrated enhanced resistance, while higher steel fiber content increased E_a at elevated sulfate concentrations, further improving durability. Importantly, the model correlates E_a and reaction rate constant with initial RPC properties such as sorptivity and permeability, reinforcing its reliability. The study also demonstrates that Na_2SO_4 concentrations above 1.1 mol/L significantly accelerate ESA damage, providing actionable insights for tailoring RPC performance in sulfate-rich environments. While the Taguchi method minimized experimental effort, future studies using full factorial designs could further validate and refine the model. This research offers a robust framework for understanding and improving the durability of RPC, contributing valuable tools for developing high-performance concrete and its performance evaluation models.

Acknowledgements Nazarbayev University funded this research under Faculty Development Competitive Research No. 201223FD8803. The authors are grateful for this support. Any opinions, findings, conclusions, or recommendations expressed in this material are those of the author(s) and do not necessarily reflect the views of Nazarbayev University. The authors also would like to thank Eldar Sharafutdinov, a laboratory coordinator at the Department of Civil and Environmental Engineering, Nazarbayev University, for his assistance in the laboratory.

Competing interests The authors declare that they have no competing interests.

References

1. Zhu P, Zhu Y, Qu W, Xie L. Stress–strain relationship for reactive powder concrete with recycled powder under uniaxial compression. Frontiers of Structural and Civil Engineering, 2024, 18(7): 1015–1027
2. Bakhbergen U, Shon C S, Zhang D, Kryzhanovskiy K, Kim J R. Assessment of reactive powder concrete subjected to three different sodium sulfate concentrations: Compressive strength, absorption, porosity, microstructure, and durability. Construction and Building Materials, 2022, 325: 126804
3. Abbas S, Nehdi M L, Saleem M A. Ultra-high performance concrete: Mechanical performance, durability, sustainability and implementation challenges. International Journal of Concrete Structures and Materials, 2016, 10: 271–295
4. El-Tair A, Youssef P, El-Nemr A. Using GLP as partial replacement in cement mortars. In: Proceedings of the MATEC Web of Conferences 199 and International Conference on Concrete Repair, Rehabilitation and Retrofitting (ICCRRR 2018). Les Ulis: EDP Sciences, 2018
5. Bektimirova U, Mukhammedrakhym I, Shon C S, Zhang D, Kim J. Effect of aggregate packing on strength of reactive powder concrete: Modeling and experimental evaluation. Materials Science Forum, 2020, 998: 299–304
6. Abbas S, Soliman A M, Nehdi M L. Exploring mechanical and durability properties of ultra-high performance concrete incorporating various steel fiber lengths and dosages. Construction and Building Materials, 2015, 75: 429–441
7. Amgad J, Hammad N, El-Nemr A M. Correlation of non-destructive with mechanical tests for self-compacting concrete (SCC). In: Proceedings of the JIC Smart Cities 2019: Joint International Conference on Design and Construction of Smart City Components. Cham: Springer Cham, 2021
8. Song H, Chen J. A time–space porosity computational model for concrete under sulfate attack. Frontiers of Structural and Civil Engineering, 2023, 17(10): 1571–1584
9. Neville A. The confused world of sulfate attack on concrete. Cement and Concrete Research, 2004, 34(8): 1275–1296
10. Liang N, Mao J, Yan R, Liu X, Zhou X. The damage evolution behavior of polypropylene fiber reinforced concrete subjected to sulfate attack based on acoustic emission. Frontiers of Structural and Civil Engineering, 2022, 16(3): 316–328
11. Negm A A, Nemr A E, Elgabbas F, Khalaf M A. High and normal strength concrete using grounded vitrified clay pipe (GVCP). Cleaner Materials, 2022, 5: 100107
12. Menéndez E, Matschei T, Glasser F P. Sulfate attack of concrete. In: Alexander M, Bertron A, de Belie N, eds. Performance of Cement-Based Materials in Aggressive Aqueous Environments. Dordrecht: Springer Dordrecht, 2013, 7–74
13. Lothenbach B, Bary B, Le Bescop P, Schmidt T, Leterrier N. Sulfate ingress in Portland cement. Cement and Concrete Research, 2010, 40(8): 1211–1225
14. Ikumi T, Cavalaro S H P, Segura I. The role of porosity in external sulphate attack. Cement and Concrete Composites, 2019, 97: 1–12
15. Bakhbergen U, Shon C S, Zhang D, Ryeol Kim J, Liu J. Optimization of mixture parameter for physical and mechanical properties of reactive powder concrete under external sulfate attack using Taguchi method. Construction and Building Materials, 2022, 352: 129023
16. Akiiz F, Tiirker F, Koral S, Yiizer N. Effects of sodium sulfate concentration on the sulfate resistance of mortars with and without silica fume. Cement and Concrete Research, 1995, 25(6): 1360–1368
17. Sarkar S, Mahadevan S, Meeussen J C L, van der Sloot H, Kosson D S. Numerical simulation of cementitious materials degradation under external sulfate attack. Cement and Concrete Composites, 2010, 32(3): 241–252
18. Tixier R L, Mobasher B. Modeling of damage in cement-based materials subjected to external sulfate attack II: Comparison with experiments. Journal of Materials in Civil Engineering, 2003,

15(4): 314–322
19. Bary B, Leterrier N, Deville E, Bescop P L. Coupled chemo-transport-mechanical modelling and numerical simulation of external sulfate attack in mortar. Cement and Concrete Composites, 2014, 49: 70–83
20. Cefis N, Comi C. Chemo-mechanical modelling of the external sulfate attack in concrete. Cement and Concrete Research, 2017, 93: 57–70
21. Kunther W, Lothenbach B, Scrivener K L. On the relevance of volume increase for the length changes of mortar bars in sulfate solutions. Cement and Concrete Research, 2013, 46: 23–39
22. Bary B. Simplified coupled chemo-mechanical modeling of cement pastes behavior subjected to combined leaching and external sulfate attack. International Journal for Numerical and Analytical Methods in Geomechanics, 2008, 32(14): 1791–1816
23. Tixier R L, Mobasher B. Modeling of damage in cement-based materials subjected to external sulfate attack I: Formulation. Journal of Materials in Civil Engineering, 2003, 15(4): 305–313
24. Flatt R J, Scherer G W. Thermodynamics of crystallization stresses in DEF. Cement and Concrete Research, 2008, 38(3): 325–336
25. Scherer G W. Stress from crystallization of salt. Cement and Concrete Research, 2004, 34(9): 1613–1624
26. ASTM C1012/C1012M-18b. Standard Test Method for Length Change of Hydraulic-Cement Mortars Exposed to a Sulfate Solution. West Conshohocken, PA: ASTM, 2018
27. ASTM C1437-20. Standard Test Method for Flow of Hydraulic Cement Mortar. West Conshohocken, PA: ASTM, 2020
28. ASTM C1585-20. Standard Test Method for Measurement of Rate of Absorption of Water by Hydraulic-Cement Concretes. West Conshohocken, PA: ASTM, 2020
29. ASTM C642-21. Standard Test Method for Density, Absorption, and Voids in Hardened Concrete. West Conshohocken, PA: ASTM, 2021
30. Alkaysi M, El-Tawil S, Liu Z, Hansen W. Effects of silica powder and cement type on durability of ultra high performance concrete (UHPC). Cement and Concrete Composites, 2016, 66: 47–56
31. El-Gazzar M, Elnemr A. Exploring the different stages of treated wastewater on various cement types. Innovative Infrastructure Solutions, 2024, 9(5): 153
32. Lv X, Dong Y, Wang R, Lu C, Wang X. Resistance improvement of cement mortar containing silica fume to external sulfate attacks at normal temperature. Construction and Building Materials, 2020, 258: 119630
33. Kumar S, Kameswara Rao C V S. Effect of sulfates on the setting time of cement and strength of concrete. Cement and Concrete Research, 1994, 24(7): 1237–1244
34. Zou D, Zhang M, Qin S, Liu T, Tong W, Zhou A, Jivkov A. Calcium leaching from cement hydrates exposed to sodium sulfate solutions. Construction and Building Materials, 2022, 351: 128975
35. Santhanam M, Cohen M D, Olek J. Modeling the effects of solution temperature and concentration during sulfate attack on cement mortars. Cement and Concrete Research, 2002, 32(4): 585–592
36. Hammad N, El-Nemr A, Hasan H E D. The performance of fiber GGBS based alkali-activated concrete. Journal of Building Engineering, 2021, 42: 102464
37. Hammad N, El-Nemr A M, Hassan H E D. Flexural performance of reinforced Alkali-activated concrete beams incorporating steel and structural macro synthetic polypropylene fiber. Construction and Building Materials, 2022, 324: 126634
38. Lubell S K, Adam S. Influence of specimen size and fiber content on mechanical properties of ultra-high-performance fiber-reinforced concrete. ACI Materials Journal, 2012, 109(6): 675–684
39. Jakob C, Jansen D, Dengler J, Neubauer J. Controlling ettringite precipitation and rheological behavior in ordinary Portland cement paste by hydration control agent, temperature and mixing. Cement and Concrete Research, 2023, 166: 107095
40. Chen B, Kuznik F, Horgnies M, Johannes K, Morin V, Gengembre E. Physicochemical properties of ettringite/meta-ettringite for thermal energy storage: Review. Solar Energy Materials and Solar Cells, 2019, 193: 320–334